AIAA Applied Aerodynamics Conference, AIAA AVIATION Forum 2017, 5 - 9 June 2017, Denver, Colorado, USA
Paper number: AIAA 2017-4464
DOI:10.2514/6.2017-4464

Undercarriage drag predictions for a Scottish Aviation Bulldog 120 light aircraft

C J Bennett, N J Lawson, J E Gautrey

National Flying Laboratory Centre
School of Aerospace, Transport and Manufacturing
Cranfield University

C.J.Bennett@Cranfield.ac.uk

Abstract

The following paper presents undercarriage drag predictions for a light aircraft with fixed landing gear. A Scottish Aviation Bulldog 120, operated by the National Flying Laboratory Centre (NFLC) at Cranfield University, is considered as the test case for this study. Taking advantage of a recently developed laser scanned model, computational fluid dynamics (CFD) techniques are exploited to investigate the undercarriage drag. Results via standard theoretical and empirical methods are compared to the CFD results. It is found that the established empirical methods matched the CFD predictions to within the stated error bands for moderate angles of attack. However, due to the aircraft flow field at higher angles of attack, some discrepancies in the level of drag predicted are observed. Further flight test data is recommended to confirm these findings.

I. Introduction

The aerodynamic drag associated with an aircraft's undercarriage, particularly in the case of non-retractable landing gear, is important to understand for a number of reasons. Since the undercarriage is fixed, it significantly affects the lift and drag characteristics of the aircraft for the duration of any given flight. Generally, the effects of the undercarriage are difficult to isolate in flight-test conditions and therefore theoretical, empirical and computational techniques are required in order to quantify them. The aim of this paper is to analyse the undercarriage drag using CFD methods in order to compare the results to standard and well accepted empirical methods [1] from the literature, as well as classic experimental studies [2, 3].

The National Flying Laboratory Centre (NFLC) at Cranfield University operates a Scottish Aviation Bulldog for research and student demonstration purposes. A recent laser scan of the Bulldog [4] has resulted in a full aircraft CFD model. The increased detail of the model, see Fig. 1, as compared to the previous CATIA half model [5], is expected to improve the correlation between CFD results and flight test data. It is worth noting that in the prior publication regarding the same aircraft [5], the authors mainly attributed the discrepancies in CFD results with respect to flight test data to the absence of the undercarriage. The undercarriage was by far the largest omission from the model in terms of size and surface area. The authors therefore utilised the ESDU undercarriage drag prediction method [1] to quantify the deficit in drag due to the undercarriage.

To analyse the accuracy of the CFD results, predictions for the undercarriage drag can be made via standard theoretical and empirical methods, the most commonly used of which is the ESDU method [1] mentioned above. Given a few basic dimensions, the ESDU method allows the overall drag coefficient for any given undercarriage to be found simply and efficiently, with a

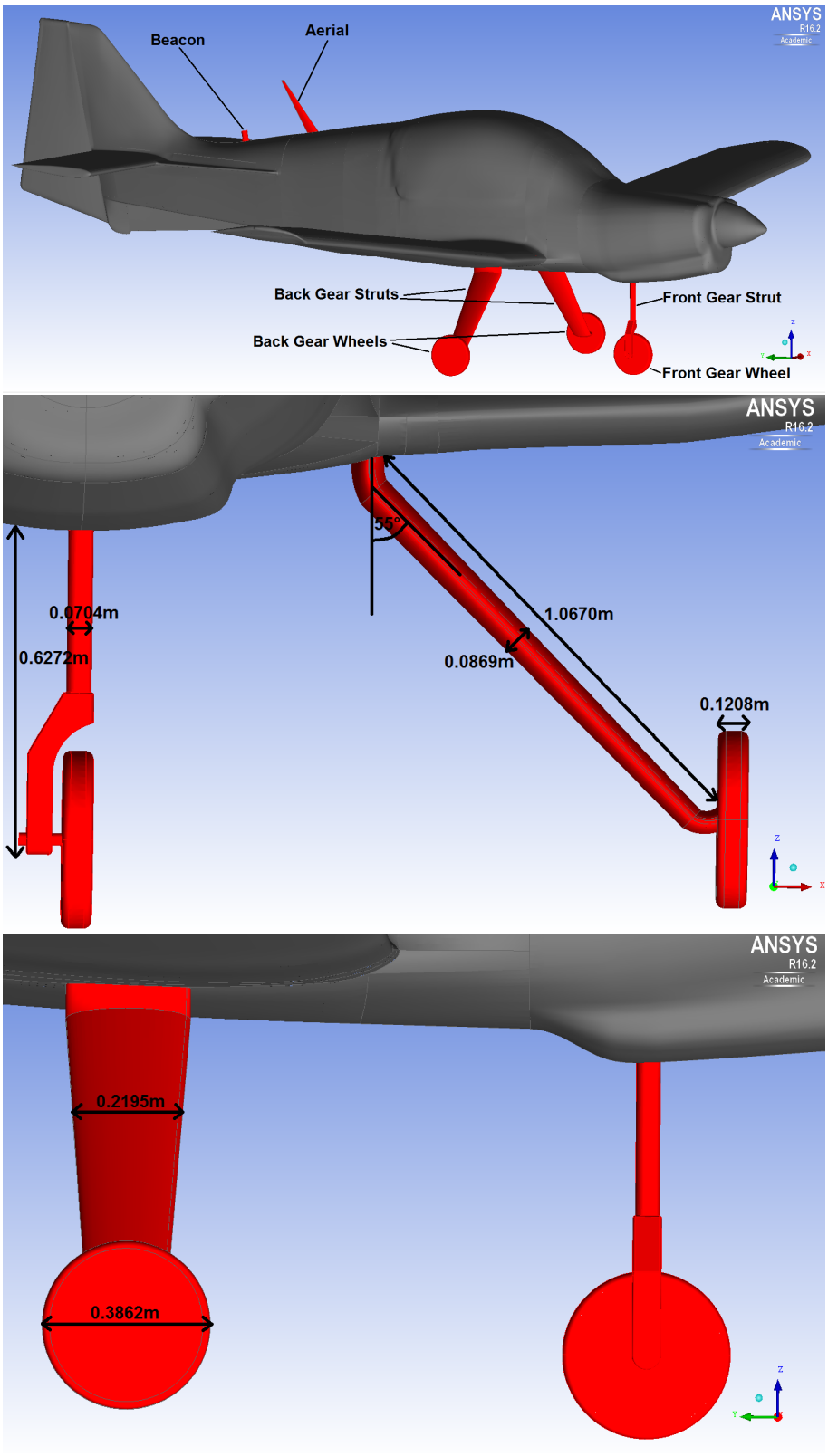

Figure 1: *New CFD model of the Bulldog (upper) and dimensions of the undercarriage (lower).*

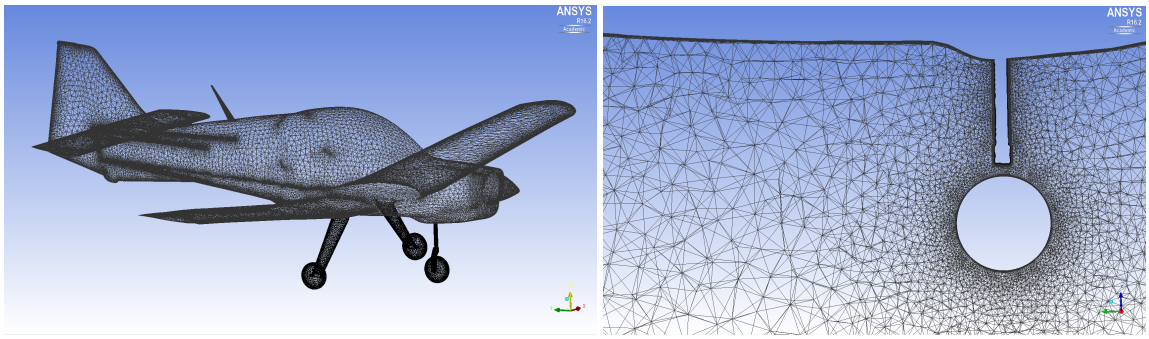

Figure 2: *Full aircraft model mesh (left) and mesh refinement surrounding the undercarriage (right).*

quoted accuracy of 30%. The ESDU approach aims to encompass all undercarriage styles and configurations, by using a a number of equations to calculate drag coefficients and correction factors based on the geometry and Reynolds number. It should be noted however, that although the ESDU document provides correction factors for inclination angles and wing proximity, it neglects other external effects, for example the pressure gradient imposed by the proximity of the fuselage. Therefore, understanding the difference in drag of both the undercarriage in free air and in the presence of the full aircraft is key to this study. To quantify these discrepancies, data gathered from a full matrix of CFD simulations is used to determine the effectiveness of the ESDU method [1], as well as other well known empirical methods, for the case of the Bulldog.

II. CFD models, methods, and verification via flight test

In the case of the ESDU approach, and similarly for other empirical methods, the total undercarriage drag is estimated by summing the drag on each individual component. Therefore for direct comparison, CFD models for the full aircraft, as well as all individual undercarriage components, were required. In addition to the full aircraft model, separate models for the main gear struts, main gear wheels, nose gear strut and nose gear wheel were individually constructed. Solutions for all cases were obtained from CFD simulations using the following methodology.

Using ANSYS ICEM CFD, the topology of all models is checked and cleaned to ensure the integrity of all surfaces before meshing. Several hybrid meshes with varying levels of detail (1-9 million cells) were generated for each model using the Octree volume meshing algorithm, in conjunction with the prism layer generator. Fig. 2 shows an example mesh with refinement on and around the undercarriage. To capture the characteristics of the boundary layer, particularly at the higher Reynolds number cases, 12 prism layers are specified at a growth ratio of 1.2 starting from an initial cell height of $0.3mm$. The range of Reynolds numbers considered here, $\mathrm{Re} \approx 2.2 - 4.1 \times 10^6$, based on the average wing chord of $1.145m$, and corresponding Mach number range, $\mathrm{M} \approx 0.1 - 0.2$, yield a non-dimensional wall distance range of $y_+ = 21 - 37$. For each mesh, the quality and integrity is analysed using the ICEM CFD mesh checking and repair tools. For each of the resulting meshes, less than 0.2% of the total elements attained a quality of 0.3 or less.

In Fluent v16.2, flow direction vectors and corresponding parameters were specified using the standard direction cosine matrix for a (1, 2, 3) Euler angle sequence to consider a full range of angles of attack from 3.4° to 11.4° so that direct comparisons to existing flight test data [5] could be made. All simulations were initiated with the Fluent set-up as summarised in Table 1. Reference values were taken directly from the aircraft manual, and flight conditions were chosen

Flight conditions and Aircraft reference values	
Altitude, (ft)	7000
Air density, ρ, (kg/m)	0.9936
Air Viscosity, ν, (kg/m-s)	1.721×10^{-5}
Air Pressure, P, (PA)	78185
Air Temperature, T, (K)	274.15
Wing Reference Area, S, (m^2)	12.02
Solver	Reynolds Averaged Navier-Stokes (RANS)
Formulation	Implicit
Type	Density Based
Time	Steady
Spatial Discretization	
Gradient	Least Squares Cell Based
Flow	Second Order Upwind
Modified Turbulent Viscosity	Second Order Upwind
Fluid Properties	
Density, ρ	Ideal gas
Viscosity, ν	Sutherland Law
Boundary Conditions	
Airframe Parts	Wall
Domain Boundaries	Pressure Far-Field

Table 1: *Summary of the Fluent set-up.*

to simulate the flight test conditions [5].

Convergence of the solutions was typically obtained within 5000-8000 iterations in all cases, the criteria of which is based on the root mean square (RMS) variance of the lift and drag monitors. It has been shown that a RMS difference of less than 10^{-5} satisfactorily determines convergence for this type of application [6].

Coarse, medium, fine, and blended[1] meshes were tested for both high and low angles of attack in order to understand the dependency of the mesh density on the drag characteristics of the model. Table 2 summarises the analysis of the drag coefficients for various mesh densities. It is seen that the blended mesh captures the overall drag characteristics of the aircraft to within 2% compared to the fine mesh. The blended mesh also predicts an undercarriage drag coefficient to within 0.5% compared to the fine mesh. Furthermore, the blended mesh is less computationally expensive compared with the fine mesh as there is a reduction of over 5 million cells. Since the undercarriage and its interaction with the main aircraft body is the focus for this study, computational expense is spared by specifying a lower resolution on areas of less interest. Hence, the blended mesh was selected as the most appropriate with which to proceed.

In obtaining the final results via the predetermined mesh, the Fluent mesh adaptation tool is used to automatically update the mesh in poorly refined areas, based on the gradient of velocity, to further increase the accuracy. This process was repeated until the converged drag coefficient is less than 5% different to the previous adaptation.

Having chosen an appropriate mesh, a number of different turbulence models were tested for

[1]The blended mesh has fine detail on the undercarriage components and under-belly of the fuselage, but coarse resolution elsewhere

Mesh	AoA (°)	No. of Cells (millions)	C_D Total	% Diff to Fine Mesh	C_D Undercarriage	% Diff to Fine Mesh
Coarse	3.4	7.9	0.0759	-2.4	0.0114	+2.7
Coarse	11.4	7.8	0.1784	-0.8	0.0162	-1.2
Medium	3.4	12.6	0.0785	+0.9	0.0119	+7.2
Medium	11.4	12.6	0.1801	+0.1	0.0167	+1.8
Fine	3.4	14.4	0.0778	-	0.0111	-
Fine	11.4	14.4	0.1799	-	0.0164	-
Blended	3.4	9.3	0.0762	-2.1	0.0110	-0.4
Blended	11.4	9.3	0.1785	-0.8	0.0163	-0.7

Table 2: *Summary of drag coefficients for varying mesh densities.*

Turb Model (No. of Equations)	AoA (°)	C_D Total	% Diff to Transitional SST	C_D Undercarriage	% Diff to Transitional SST
Spalart-Allmaras (1)	3.4	0.0757	+0.9	0.0109	-1.8
Spalart-Allmaras (1)	11.4	0.1775	-2.0	0.0159	-3.0
$k-\epsilon$ Realisable (2)	3.4	0.0734	-2.1	0.0113	+1.5
$k-\epsilon$ Realisable (2)	11.4	0.1752	-3.3	0.0150	-8.5
$k-\omega$ SST (2)	3.4	0.0750	0.0	0.0110	-0.9
$k-\omega$ SST (2)	11.4	0.1823	+0.7	0.0176	+7.3
Transitional SST (4)	3.4	0.0750	-	0.0111	-
Transitional SST (4)	11.4	0.1811	-	0.0164	-

Table 3: *Summary of drag coefficients obtained via various turbulence models.*

both low and high angle of attack cases. These range from the 1-equation Spalart-Allmaras model to the 4-equation Transitional SST model. Table 3 summarises the analysis of the drag coefficients for the various turbulence models. Considering the 4-equation Transitional SST model as the benchmark case, it is seen that the more complex models do not justify the added computational expense. The 1-equation Spalart-Allmaras model yields results accurate to within 3% for both the full aircraft C_D and the undercarriage drag characteristics. Hence, the Spalart-Allmaras turbulence model was chosen to be used for the full matrix of CFD simulations.

Following this refinement process, the resulting CFD model (Model 2) was compared to flight test data [5] and also to results from the previous CATIA half model (Model 1) [5], see Fig. 3 and Table 4 where values of the zero-lift drag, C_{D0}, and the lift induced drag correction factor, K, are summarised. Since Models 1 and 2 do not include the propeller and it's effects, the CFD simulation conditions are most representative of the glide flight test data.

It is seen that Model 2 predicts the zero-lift drag of the glide flight test results to within 2% as compared to over 50% for Model 1. However, the K value for Model 2 is 20% lower than for the glide flight test data, meaning that for higher angles of attack Model 2 under predicts the drag coefficient. This deficiency could be explained by the propeller blades: although not spinning during the glide flight test, the propeller blades still contribute to the overall drag on the aircraft.

Despite this, it is seen that Model 2 significantly improves the accuracy of the CFD results as compared to Model 1. As discussed above, the improved accuracy is mainly attributed to the inclusion of the undercarriage, aerials, beacon, and other general detailing of the newly developed

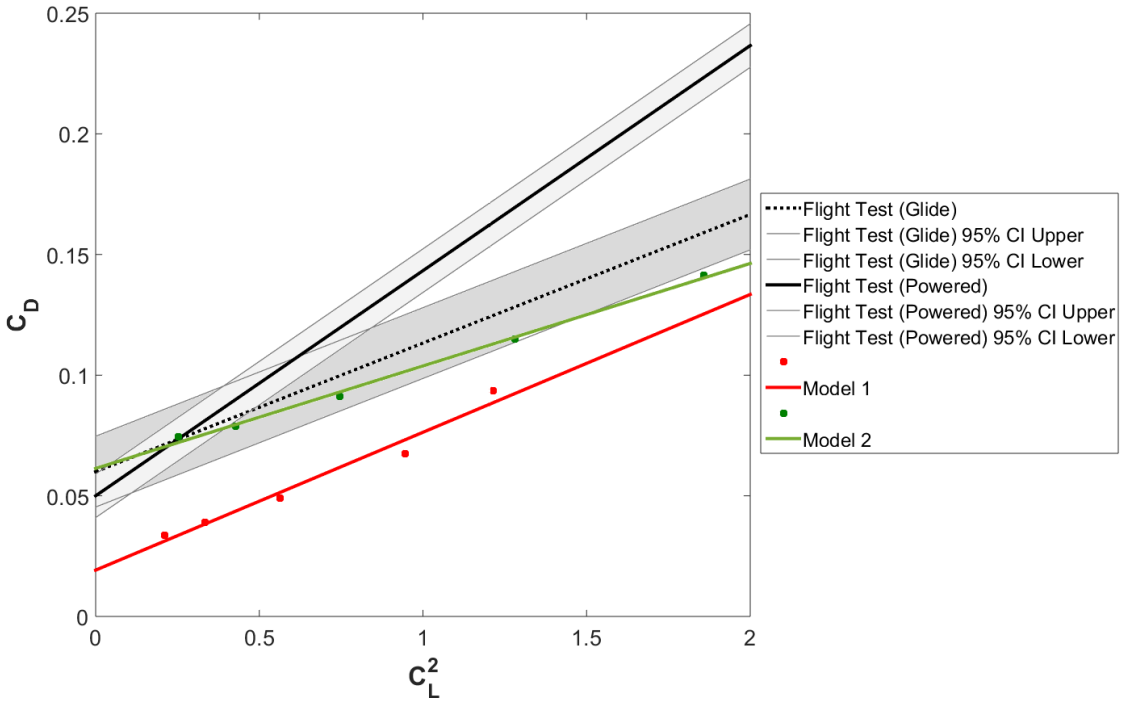

Figure 3: *CFD model comparison to flight test data with 95% confidence intervals (shaded bands).*

	C_{D0}	K
Flight Test - Glide	0.0600	0.0533
Flight Test - Powered	0.0500	0.0933
Model 1	0.0192	0.0571
Model 2	0.0613	0.0425

Table 4: *Comparison of the zero-lift drag and lift induced drag correction factor for flight test and CFD results.*

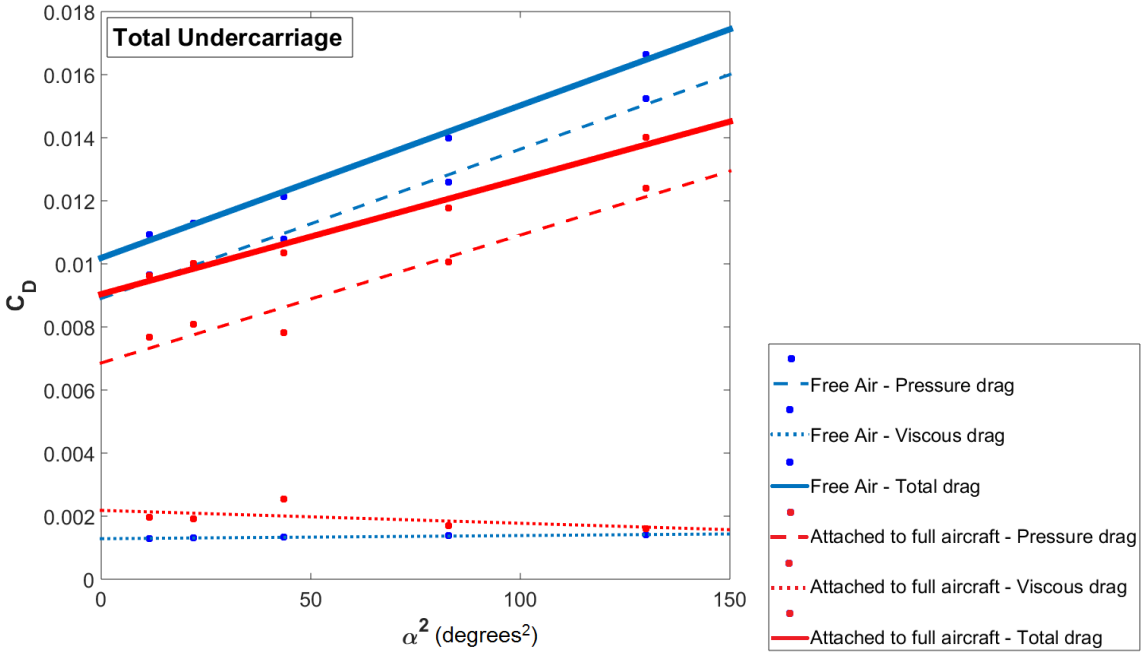

Figure 4: *CFD results comparing the total undercarriage drag coefficient for cases where the undercarriage is considered in free air and also attached to the full aircraft.*

model.

III. CFD Results

The drag characteristics of the undercarriage when attached to the full model and in free air are now analysed in detail. A drag polar for both scenarios is given in Fig. 4.

The first observation to make (see Fig. 4) is that the total undercarriage drag is greater when the components are considered in free air. This is an important finding since the theoretical drag prediction methods, which are discussed in detail in a later section, typically consider undercarriage components in isolation, before applying a correction to the undercarriage components which are in the immediate vicinity of the wings only. It is seen from Fig. 5, where the undercarriage parts and drag coefficients components are separated, that the viscous drag in all cases remains approximately unchanged in both free air and full aircraft configurations. However, for all undercarriage components it is seen that in free air the pressure drag is considerably higher. This observation is confirmed by analysing surface flow visualisations. Fig. 6, for example, shows that a flow separation region is present on the rear of the main gear struts and wheels, but is not present when these components are attached to the full aircraft, for both low and high angles of attack. Similar observations can be made regarding the nose gear strut and wheel.

Secondly, considering Fig. 4 it is seen that in both cases the drag coefficient increases with angle of attack. Considering Fig. 5 where the individual components are separated, it is seen that this result is directly related to the shape of the main gear struts as they are the only components significantly affected by the angle of attack. The faired and tapered shape of the streamlined main gear struts mean that the drag characteristic is similar to that of an aerofoil when an angle of

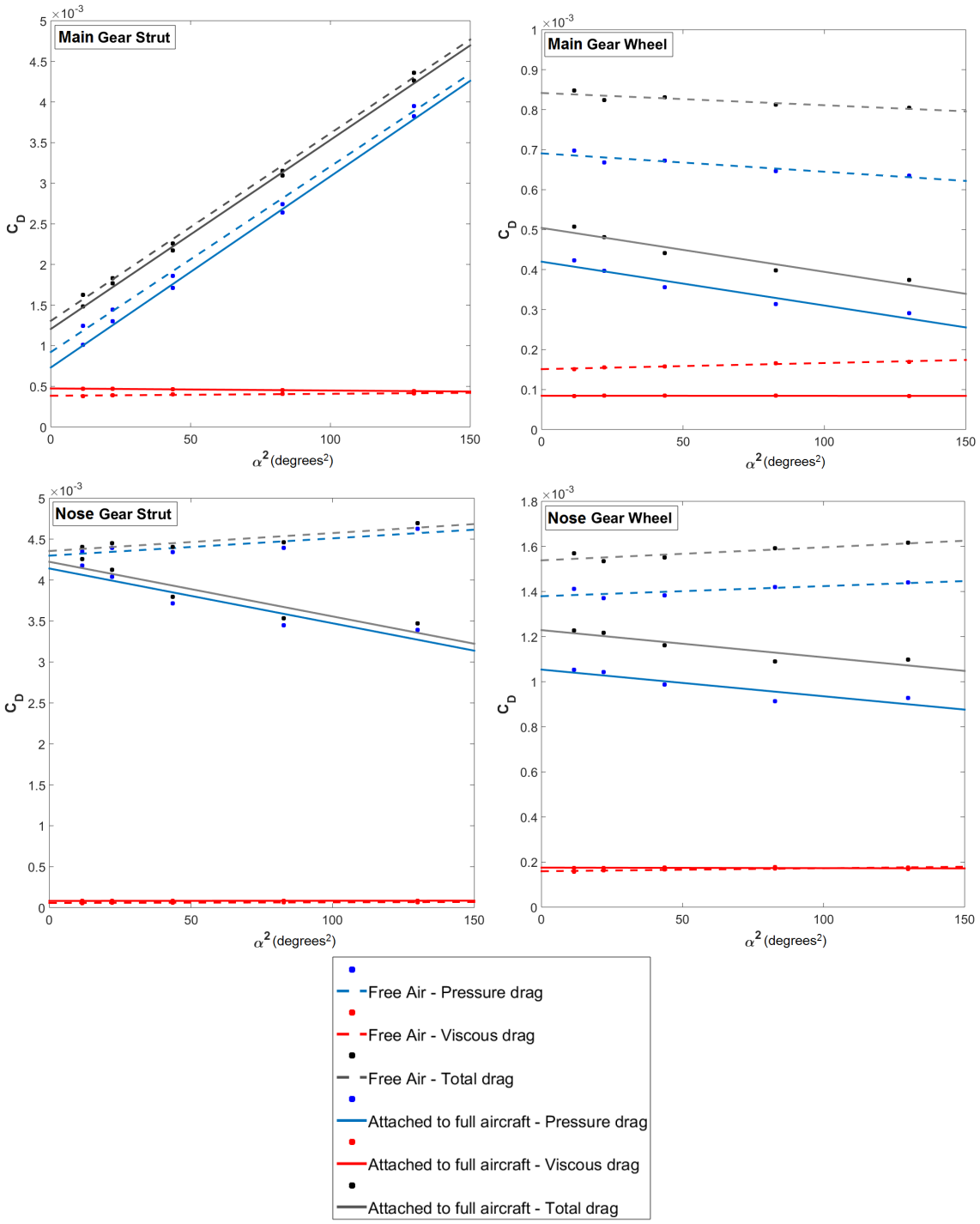

Figure 5: *Comparison of individual undercarriage component drag coefficients.*

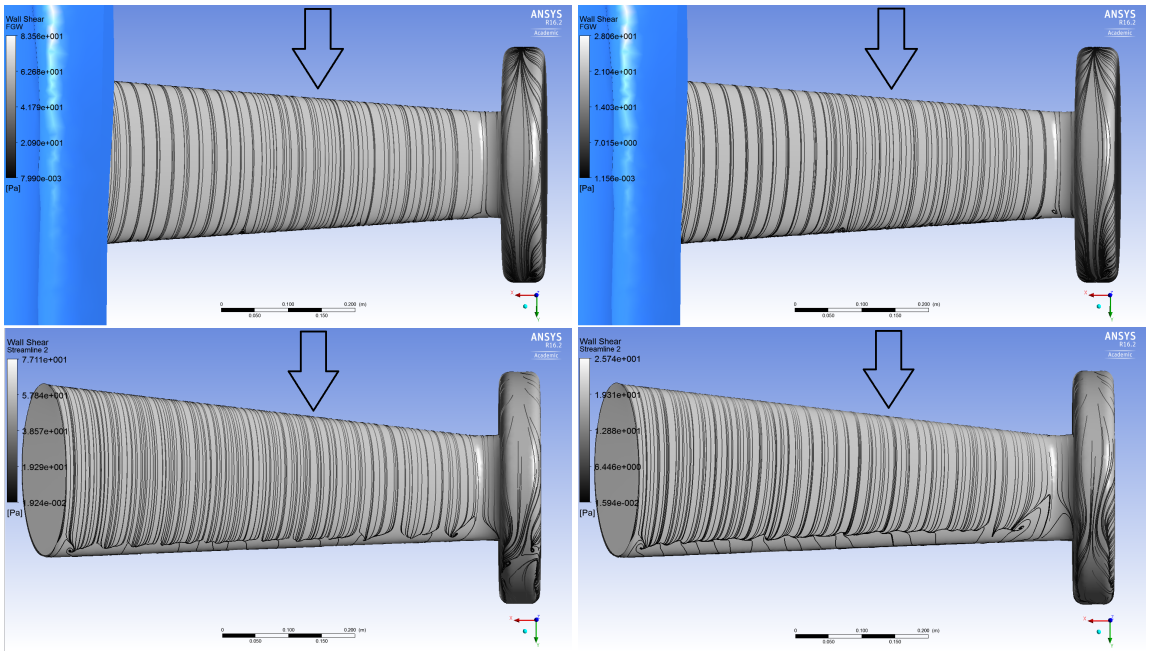

Figure 6: *Top view of the main gear strut attached to the full aircraft (top) and in free air (bottom), for 3.4° angle of attack cases (left) and 11.4° angle of attack cases (right).*

attack is applied, and can be plotted in the form of a drag polar.

Furthermore, it is seen that the effect of angle of attack is less pronounced when the undercarriage is investigated as part of the full aircraft. The presence of the wings and fuselage generate a pressure field below the aircraft, which alters the upwash angle of the on-coming flow. Analysing the flow angle immediately upstream of the struts (see Fig. 7) it is seen that in general the pressure field generated by the aircraft's lifting surfaces constrains the air flow onto the undercarriage at approximately half of the far field flow angle. This is further visualised by the streamline plots in Fig. 8.

Detailed analysis into the pressure coefficient, C_p, distribution on the undercarriage at the slice normal positions as shown in Fig. 9, is given in Fig. 10. It is confirmed that for both the nose and main gear struts, low and high angles of attack, the presence of the full aircraft affects the surface C_p along the total length of the slice normal. In the case of the main gear struts, it is seen that there is a peak C_p reduction of 52% at the highest angle of attack, and a peak C_p increase of 14% at the lowest angle of attack. In the case of the nose gear strut, it is seen that there is a peak C_p increase of 37% at the highest angle of attack, and a peak C_p increase of 73% at the lowest angle of attack. Furthermore, this effect is more pronounced the closer to the fuselage the slice position is considered. The same can be seen for the undercarriage wheels, with slice positions shown in Fig. 11. The plots corresponding to the wheels in Fig. 12 show that the differences in C_p are smaller since the wheels are further from the surface of the fuselage and lifting surfaces. In the case of the main gear wheels, it is seen that there is a peak C_p reduction of 17% at the highest angle of attack, and a peak C_p reduction of 5% at the lowest angle of attack. In the case of the nose gear wheel, it is seen that there is a peak C_p reduction of 2% at the highest angle of attack, and a peak C_p reduction of 1% at the lowest angle of attack. It should also be noted from Figs. 10 and 12 and the peak C_p value changes given above, that location of the nose and main gear with respect to

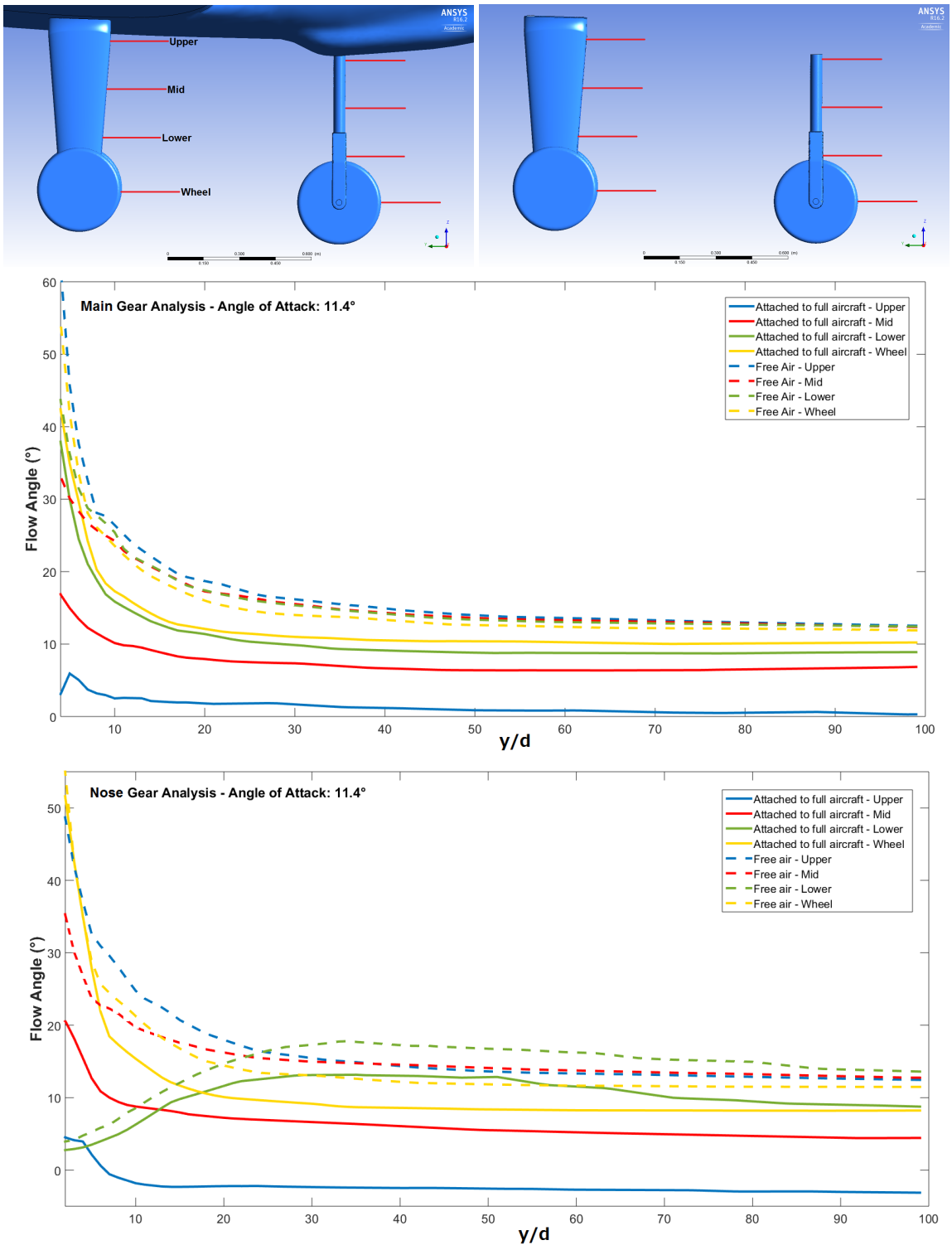

Figure 7: *Flow angle analysis.*

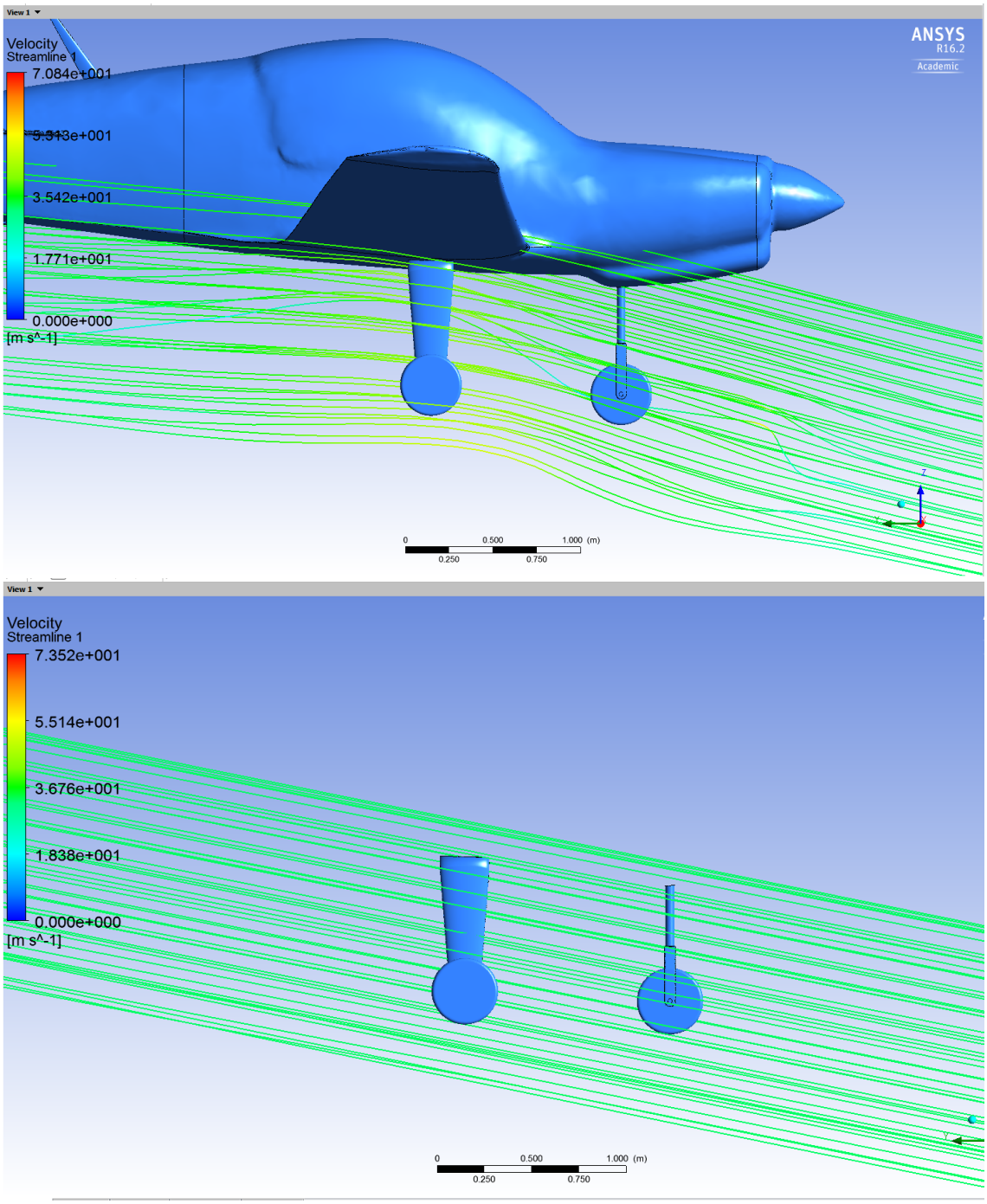

Figure 8: *Streamlines showing the air flow angle onto the undercarriage for the case of* $\alpha = 11.4^{\circ}$.

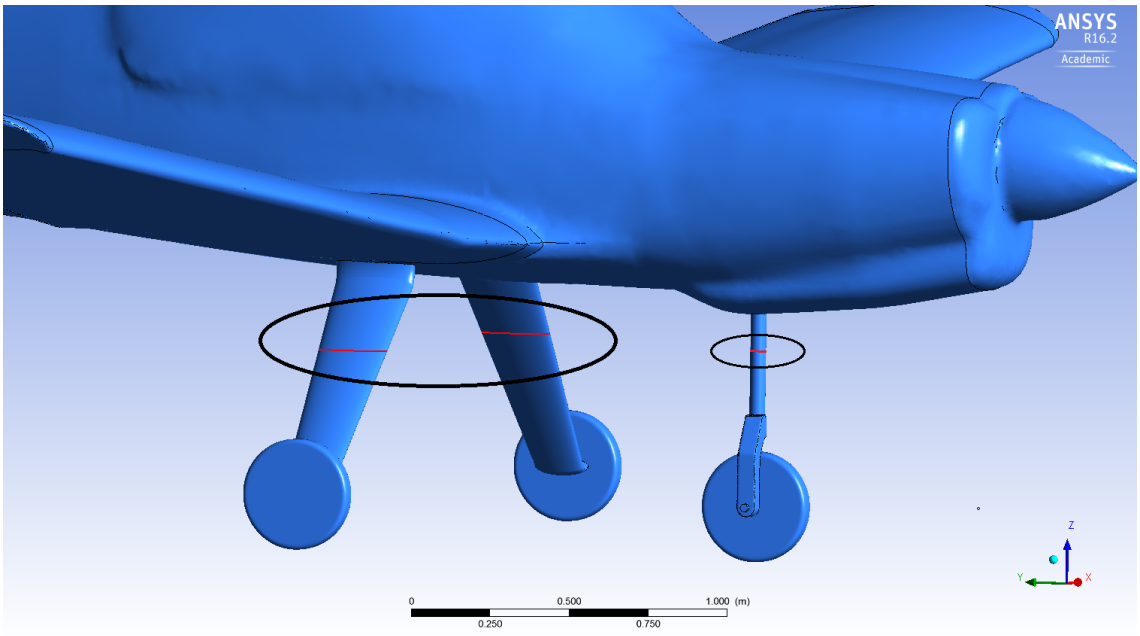

Figure 9: *Slice positions on the undercarriage struts for the C_p plots (same positions for free air cases).*

the predominant lifting surfaces of the aircraft also has a significant effect on the local pressures.

From the CFD analysis given above, it is seen that for the specific case of the Bulldog the undercarriage drag is greatly affected by the presence of the aircraft. Therefore, for best accuracy, the undercarriage must be considered as part of the full aircraft model. The following section applies the ESDU undercarriage drag prediction method to the specific case of the Bulldog, and compares the results to those found via the CFD simulations. It is shown that the ESDU prediction, neglecting the influence of the full aircraft, is most comparable to the CFD results when undercarriage parts are considered in free air.

IV. ESDU drag prediction method compared to CFD results

ESDU 79015 [1] is the most widely acknowledged empirical method for calculating undercarriage drag. The main advantage of the method is that basic estimations can be obtained if a number of key dimensions are known. Furthermore, correction factors for inclination angles allow a range of angles of attack to be considered. The drag coefficients of individual undercarriage parts are calculated separately using the appropriate equations and then summed to find the total.

It is assumed for the initial ESDU calculations that the undercarriage components are positioned normal to the on-coming air flow, and are in isolation from other aircraft parts, namely the main aircraft body. Following this, correction factors for inclination angles are applied to the struts, and the correction factor for wing proximity is applied to the main gear since it is fixed directly below the wings.

All dimensions of the Bulldog undercarriage for the implementation of the ESDU method are taken from the laser scan of the aircraft, eliminating any errors due to the scanning process [4]. This ensures that both the CFD model and the ESDU method are applied using the exact same dimensions. However, some assumptions and approximations have to be made regarding the

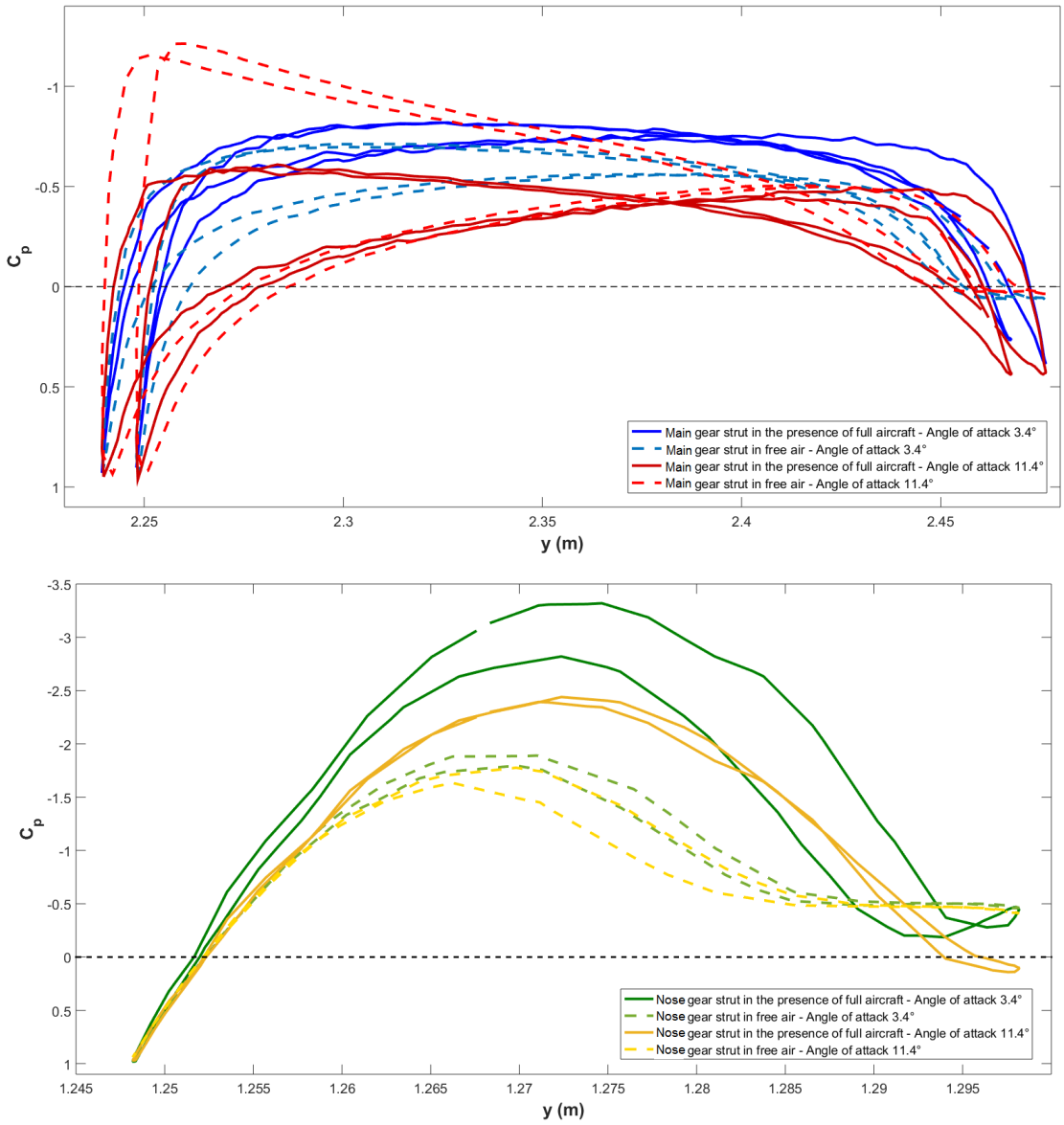

Figure 10: *Cp plots for the undercarriage struts.*

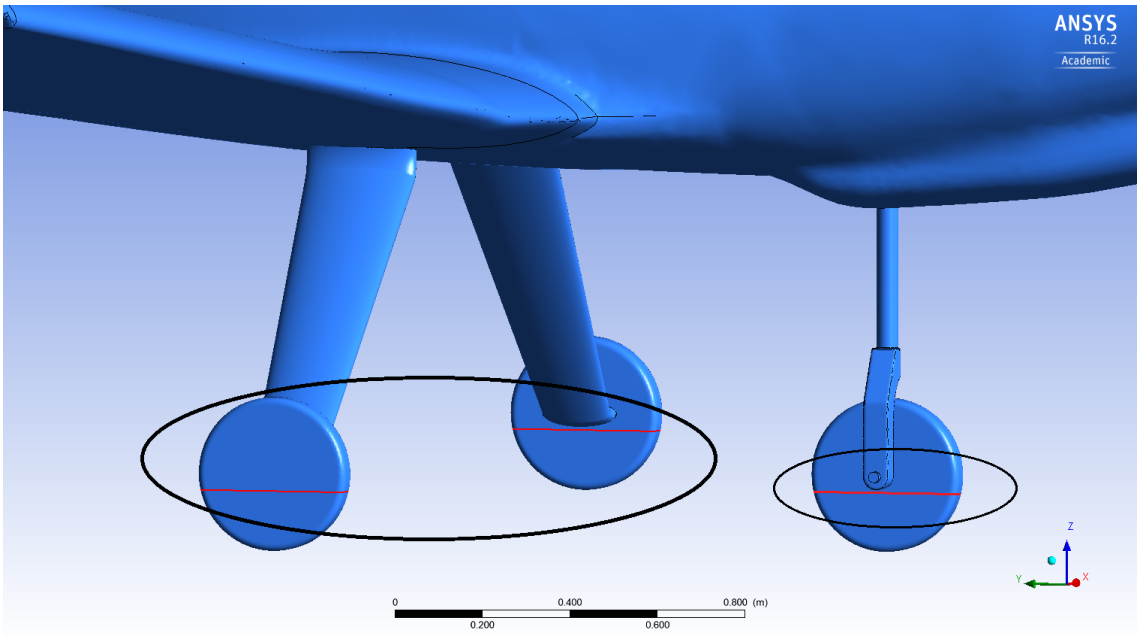

Figure 11: *Slice positions on the undercarriage wheels for the C_p plots (same positions for free air cases).*

dimensions in order to apply specific equations. For example, the geometry of some parts are simplified so that they can be treated as either cylindrical or streamlined sections with averaged dimensions. The dimensions of the Bulldog undercarriage are shown in Fig. 1.

Thus, by considering each individual wheel and strut separately before summing the components, leads to

$$C_{DU} = C_{Dw} + C_{Ds}, \tag{1}$$

where C_{DU} is the total undercarriage drag component, C_{Dw} is the total wheel drag components and C_{Ds} is the total strut drag components.

Considering a single Bulldog wheel drag coefficient:

$$C_{Dw} = \frac{D_w}{qS} = \frac{C_D}{C_{D0}} C_{D0} \frac{bd_w}{S}, \tag{2}$$

where D is the drag force acting in the free stream direction, q is the dynamic pressure, S is the aircraft reference area (in this case, the whole aircraft area $S = 12.02 m/s^2$), b is the width of the wheel and d is the diameter of the wheel. Subscript w corresponds to variables relating to the wheels. The ratio C_D/C_{D0} is found from Fig. 1 [1] based on the ratio d_w/b. The value C_{D0} is given depending on whether the Reynolds number associated with the wheel is sub- or supercritical. In accordance with the CFD simulations and flight tests [5], all wheel Reynolds numbers are in the supercritical region. In this case, ESDU 79015 [1] advises that the drag on a wheel increases when in the presence of a single strut attached at an angle less than 45°. This is not the case for both the nose and main gear on the Bulldog, see Fig. 1. Hence, the coefficient C_{D0} should be taken as 0.55.

Therefore, having calculated the required coefficients, the wheel drag coefficient can be found using Eqn. (2) and the dimensions given in Fig. 1,

$$C_{Dw} = (0.485 \times 0.55) \frac{(0.1208 \times 0.3862)}{12.02} = 0.001035.$$

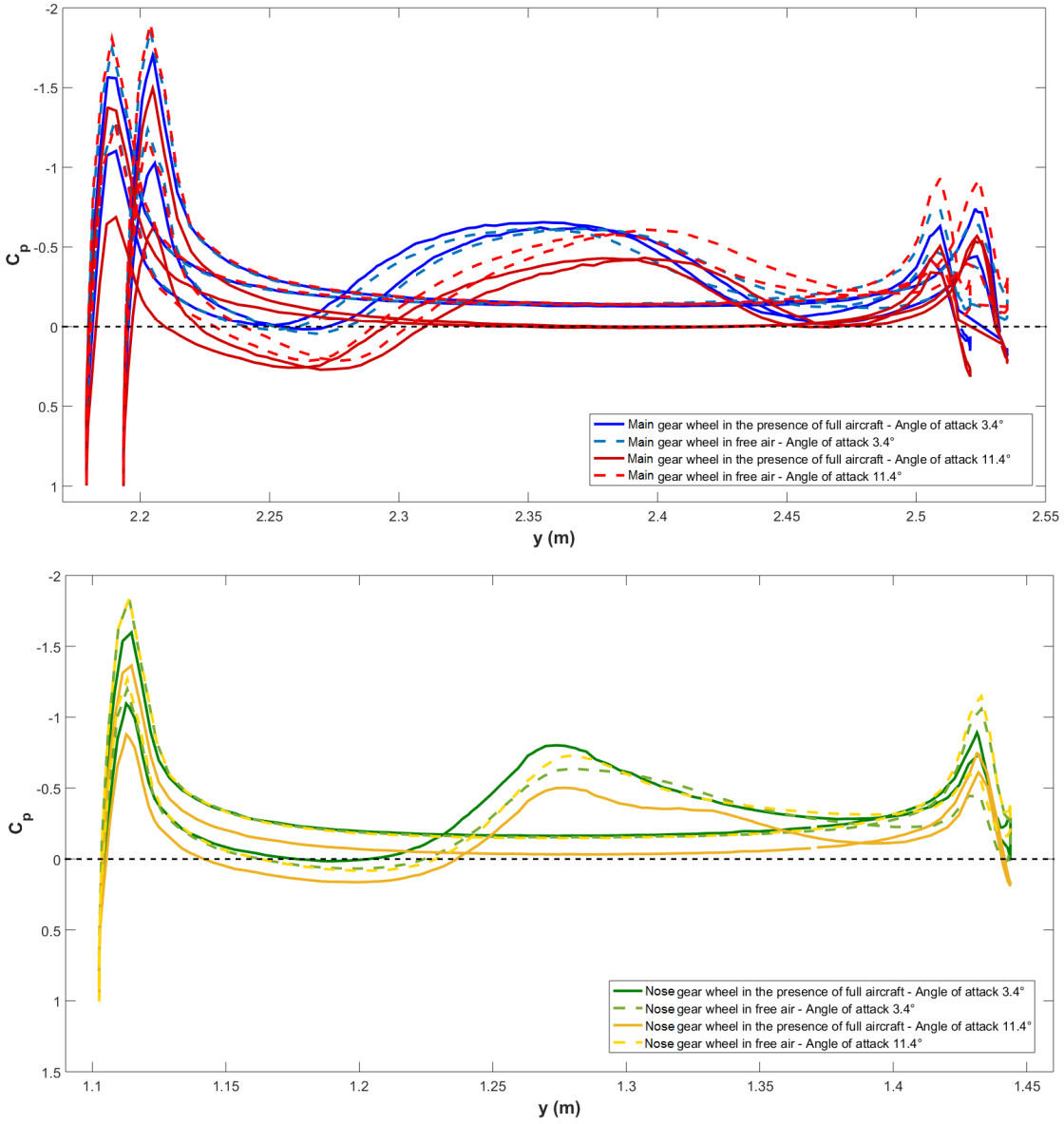

Figure 12: *Cp plots for the undercarriage wheels.*

Therefore, the total wheel drag coefficient for the Bulldog is given by

$$C_{Dw} = (3 \times 0.001035) = 0.003106. \tag{3}$$

This result is not corrected for angle of attack due to the cylindrical shape of the wheels. However, the main gear wheels are corrected for the wing proximity. Based on the wing thickness to chord ratio, and the depth of the undercarriage normal to the wings, a correction factor is applied to the main gear wheels. Fig. 13a compares wheel drag coefficients found via the ESDU method and CFD simulations. It is seen that the initial ESDU prediction is in close agreement with the CFD results when the undercarriage is considered in free air. The wing correction factor shifts the prediction closer to the CFD results for the undercarriage attached to the full aircraft, but does not compensate for the total difference. As described in the previous section, the pressure field generated by the fuselage, and the deflection of the air flow around the nose section, also have an effect on the undercarriage drag. The shaded area, as in all graphs of Fig. 13, describes a 30% error band for the ESDU prediction, as specified by ESDU [1].

Now considering the undercarriage struts, it is seen that the shape of the nose and main gear components are different and so must be treated separately. The drag coefficient for the cylindrical vertical nose gear strut is calculated via the equation

$$C_{Ds_c} = \frac{D_{s_c i}}{qS} = C_{Ds_c} \frac{l_{s_c} d_{s_c}}{S}, \tag{4}$$

where l is the length of the strut and d is the diameter. Subscript s corresponds to variables relating to the struts, and c indicates variables relating to cylindrical cross section parts. The coefficient C_{Ds_c} is obtained from a previous ESDU document regarding circular cylindrical structures [7]. Hence the drag coefficient may be calculated using Eqn. (4) and the dimensions given in Fig. 1,

$$C_{Ds_c} = 1.2 \left(\frac{0.6272 \times 0.0704}{12.02} \right) = 0.0044. \tag{5}$$

An inclination factor, $R_1 c = \cos^3 |\alpha|$, can be applied to the above result to modify the drag coefficient for variations in angle of attack, α. This allows direct comparison of the final result to the CFD results, see Fig. 13b. It is seen that the inclination factor forces the general trend of the ESDU data points downwards, as in the case of the CFD results where the undercarriage was part of the full aircraft model. However, again, the correction factor fails to compensate for the total difference in the result. Note also that the wing proximity factor is not applied here due to the nose gear position far forward of the wings.

Finally considering the streamlined main gear struts, the drag coefficient is calculated via

$$C_{Ds_s} = \frac{D_{s_s i}}{qS} = C_{Ds_s} \frac{l_{s_s} c_{s_s}}{S}, \tag{6}$$

where c is the chord and subscript s indicates variables relating to a streamlined strut. To calculate the coefficient C_{Ds_s}, alternative formulae are required depending on the logarithm of the Reynolds number associated with the strut. Hence, in accordance with the CFD simulations and the flight tests [5], the two data points obtained at the highest angles of attack should use a different formula to those obtained at the lower angles of attack. Hence, for $5 \leq \log_{10} \mathrm{Re}_{s_s} < 5.75$, $C_{D_{s_s}}$ is calculated via

$$C_{Ds_s} = 0.0084 \left(1 + \frac{t_{s_s}}{c_{s_s}} \right) + \left(\frac{t_{s_s}}{c_{s_s}} \right)^2$$

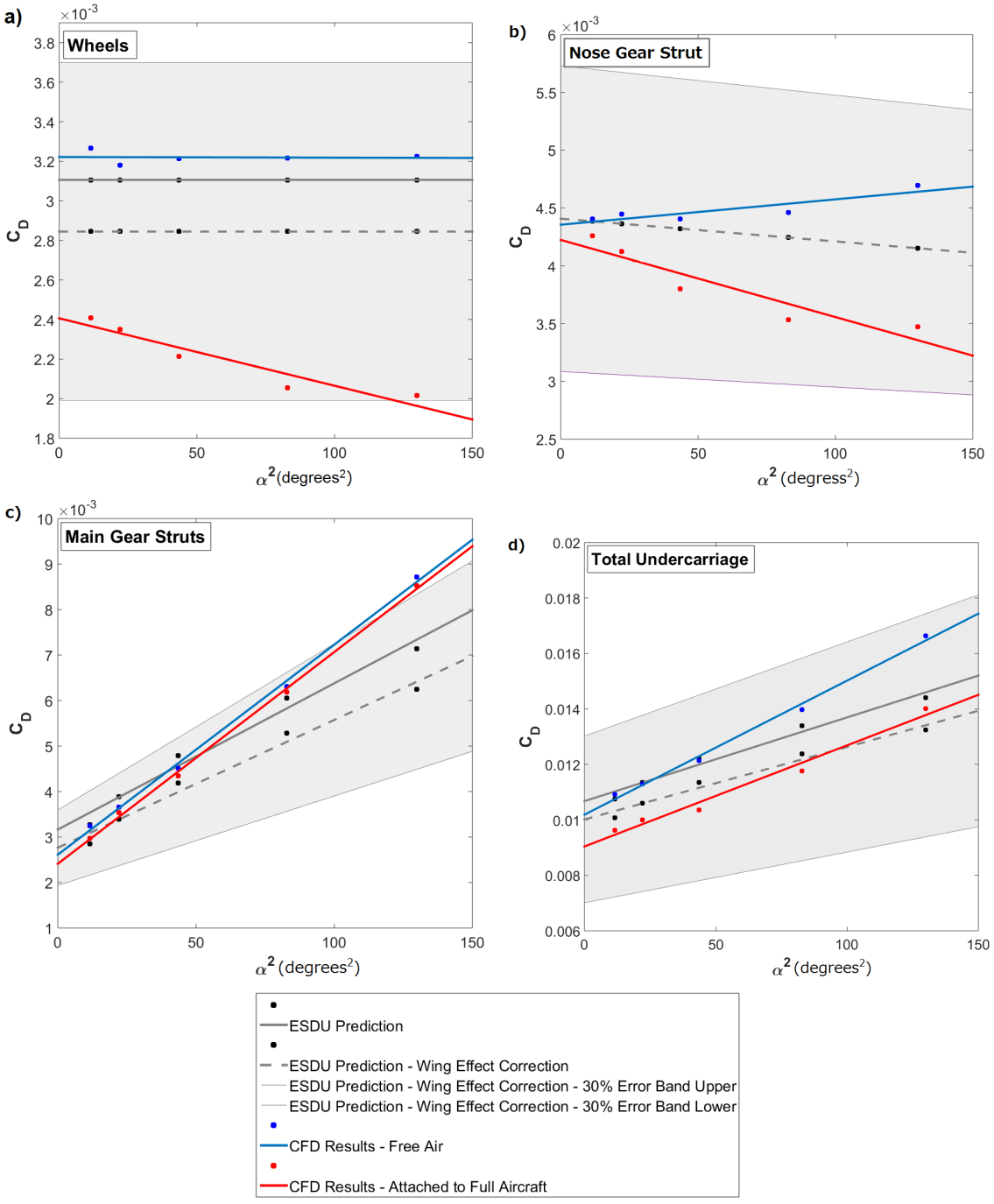

Figure 13: *Comparison of CFD and ESDU undercarriage drag predictions.*

and for $5.75 \leq \log_{10}\mathrm{Re}_{s_s} < 7.5$,

$$C_{Ds_s} = 0.00495\left(1 + 2\frac{t_{s_s}}{c_{s_s}} + 60\left(\frac{t_{s_s}}{c_{s_s}}\right)^4\right)$$

should be used, where t_{s_s} is the thickness of the streamlined strut and c_{s_s} is the chord of the streamlined strut. Hence the drag coefficient may be calculated using Eqn. (6), corresponding C_{Ds_s}, and the dimensions given in Fig. 1.

Since the main gear struts on the Bulldog are not vertical but are attached at 55°, an increase in angle of attack yields an increase in drag coefficient. The characteristic increase in drag coefficient with angle of attack for a horizontal aerofoil can be used here to approximate the increase in drag coefficient for the main gear struts. A drag coefficient correction based on Hoerner [8] for streamlined shapes of varying width to chord ratios is used to correct for angle of attack. Furthermore, the wing proximity correction factor is also applied.

The results for the main gear struts are shown in Fig. 13c. In general, the ESDU prediction is in good agreement with the CFD results for low angles of attack. However, since both sets of CFD simulations (free air cases and attached to the full aircraft) yield similar results, it is difficult to draw conclusions regarding accuracy. The shallower gradient of the line describing the ESDU prediction may be attributed to the different formulae used for the calculation of the coefficient $C_{D_{s_s}}$ since the characteristic Reynolds numbers for those specific data points crossed over the given boundaries. It is apparent that this causes the data points to fall into two distinct sets (the first three and the last two). If a line of best fit was drawn through the first three points it is seen that the gradient of the line would match more closely to the CFD results. This observation highlights the challenges in working in the vicinity of the transitional Reynolds number region.

Finally, summing the drag coefficients for the wheels and struts as in Eqn. (1) gives a total undercarriage drag coefficient depending on the angle of attack. Fig. 13d compares the ESDU method prediction with CFD results for both the undercarriage in free air and in the presence of the full aircraft. It is seen that the total undercarriage drag coefficient found via ESDU is in close agreement with the CFD results in general. However, the shallower gradient of the line representing the ESDU prediction suggests that the correction factor for inclination angles under estimates the effect of the increasing angle of attack. The correction for wing proximity does improve the prediction with respect to the CFD results for the full aircraft model but is not sufficient to compensate for the total difference. Despite this, the 30% error band of the ESDU method captures all of the CFD results.

All comparisons shown in Fig. 13 therefore suggest that the ESDU method fails to take into account the full effects of the pressure field and flow disturbances due to the presence of the full aircraft. It must be noted however that remarks regarding the accuracy of the ESDU prediction with respect to the CFD simulations are limited to the specific case of the Bulldog. Further analysis of other aircraft is required to make more general conclusions. To provide some context for the results outlined above, drag coefficient predictions via alternative empirical methods are discussed in the following section.

V. A discussion on alternative methods

Since the Bulldog undercarriage wheels and nose gear strut may be approximated as cylindrical sections, the classical literature on flows around circular cylinders may be compared to the CFD and ESDU results found in the previous section. Standard publications in the field of fluid mechanics [9, 10] discuss the drag on 2D circular cylinders of various aspect ratios as a function

of the Reynolds number. The effect of the Reynolds number transition on the drag is also well documented and so provides context for the results given here. It must be noted, however, that a cylinder of finite length has a drag coefficient smaller than that of a 2D cylinder due to the decrease in separation velocity of the side wall flow [11].

Hence, the most direct comparison for this particular study can be made to the experimental work [12] where the author presents drag coefficients for cylinders with varying length to diameter ratios in the Reynolds number range $10^4 - 10^7$. The author combines the results with previously published data to establish a comprehensive picture of the drag characteristics of circular cylinders of varying aspect ratios, for a large range of Reynolds numbers. It is seen that the largest spread of results occurs in the vicinity of the transition Reynolds number, further indicating the instability of the flow in this region. However, it is seen that in general, the drag coefficient decreases as the length to diameter ratio increases.

It is therefore possible, using the wealth of literature on the topic, to contextualise the CFD and ESDU drag predictions for the Bulldog undercarriage wheels and nose gear strut, and conclude that the magnitude of the drag coefficients calculated above are as expected. However, due to the difficulty imposed by the transitional region of the Reynolds number, and the dependency on the specific aspect ratio of any given circular cylinder, it is not possible to add to the discussion comparing the accuracy of the CFD results to the ESDU prediction since the level of accuracy already attained is greater than can be derived from the publications mentioned above.

Now considering the streamlined main gear struts, it is possible to approximate the pressure and viscous drag components separately via a number of standard techniques. Firstly, the skin friction coefficient can be approximated using a choice of several well known equations depending on whether the flow is laminar of fully turbulent. Again, since the Reynolds numbers considered here are in the transitional region, deciding upon the most applicable equation is challenging. For the higher angle of attack cases where the flight test flow velocities are lower and the flow around the undercarriage is likely to be laminar, it would seem most appropriate to use the Blasius Friction Law [13]. However, for the lower angles of attack where the flow velocities are higher and the flow around the undercarriage is more likely to be turbulent, the Schlichting empirical formula may be most applicable. Both equations approximate the skin friction coefficient as a function of the Reynolds number[2] only. There are also limitations using these predictions with respect to the required pressure gradient profiles.

To calculate the pressure drag coefficient (the main contributor to the overall drag coefficient, see Fig. 5) the form factor method [14, 15] may be used. It is seen from the equation given in [15] that the pressure drag coefficient can be approximated as a function of the skin friction coefficient, the form factor, and the wetted and reference areas of the strut[3]. Again, there are a number of equations which may be applied to calculate the form factor. Here, since the back gear strut can be treated as a streamlined object, Hoerner's method [16], which depends only on the thickness to chord ratio of the strut, is considered most appropriate.

Therefore, as with the case of the cylindrical undercarriage components, it can be remarked that the drag coefficients as predicted by the CFD and ESDU approaches are realistic compared to other commonly used empirical methods. However, it is not possible to conclude that either approach is more accurate than another. The comparison to standard literature and commonly used empirical methods is used to check the CFD and ESDU predictions.

[2]Here, the Reynolds number is calculated based on the chord length of the strut.

[3]The wetted area is the total surface area and the reference area is taken as the area of a 2D projection of the object on the ground.

VI. Conclusions

The undercarriage drag on a Scottish Aviation Bulldog 120 has been investigated in an extensive CFD study in order to compare the results to those found via standard theoretical and empirical approaches, in particular ESDU 79015 [1]. Such methods generally consider the drag on each individual undercarriage component in isolation, before summing them to find a total undercarriage drag. However, it is shown in the CFD analysis that the drag on the undercarriage is greatly affected by the presence of the full aircraft. Although, for example in the case of the ESDU method, a correction may be applied for wing proximity, it is seen that the entire aircraft shape should be taken into consideration. The angle of the oncoming flow, flow velocity, and local pressure field below the aircraft, all of which influence the undercarriage drag, are shown to be affected by the aircraft flow field.

Results were found for both undercarriage components in isolation and as part of the full aircraft model. It was seen that the viscous drag coefficient was approximately equal in both situations, but the pressure drag could differ by up to 40% at the higher angles of attack. This was confirmed by analysing the surface flow in which there was evidently more flow separation on the undercarriage when considered in isolation rather than as part of the full aircraft. Furthermore, flow angle analysis immediately forward of the undercarriage, and also surface C_p plots, solidified these findings.

For comparison of the ESDU method with the CFD results, a number of key equations were applied depending on whether the Reynolds number was sub- or super-critical. Since the range of flight conditions considered here span the region of the transitional Reynolds number, identifying the most appropriate equations was challenging. Nevertheless, the ESDU prediction matched closely with the CFD prediction, particularly when the undercarriage parts were considered in free air, as expected. The corrections which were applied to account for the inclination angle and the wing proximity did align the ESDU prediction more closely to the full aircraft CFD results, however the correction was not significant enough to compensate for the total discrepancy. Furthermore, the quoted 30% error band of the ESDU method captures almost all of the CFD results up to angles of attack of 11.4°.

Further comparisons of the CFD and ESDU results were made using classical theoretical and experimental works, as well as industry standard techniques. It is confirmed that the magnitude of the predicted drag coefficients are as expected, and the relative change based on the Reynolds number appear valid.

It is therefore concluded that the most accurate representation of the undercarriage drag characteristics is found when the undercarriage is considered as part of the full aircraft, however, further investigation regarding other aircraft is required to confirm the findings given here. In addition, more extensive flight test results focusing specifically on laminar or fully turbulent conditions would simplify the application of the ESDU method and potentially yield more comparable results. In the region of the transition, a higher density of data points is required to fully capture the flow behaviour at this specific Reynolds number. This would lead to a better understanding of the flow characteristics in the specific case discussed here.

References

[1] ESDU. Undercarriage drag prediction methods. Technical Report 79015, UK, 1987.

[2] W. H. Herrnstein and D. Biermann. The drag of airplane wheels, wheel fairings, and landing gears - I. Technical Report NACA-TR-485, Langley Memorial Aeronautical Laboratory, 1935.

[3] D. Biermann and W. H. Herrnstein. The drag of airplane wheels, wheel fairings, and landing gears - II - non-retractable and partly retractable landing gears. Technical Report NACA-TR-518, Langley Memorial Aeronautical Laboratory, 1936.

[4] S. Salmon. Reverse Engineering and Computational Aerodynamic Modelling of a Scottish Aviation Bulldog Aircraft. Master's thesis, Cranfield University, 2012.

[5] N. J. Lawson, N. Salmon, J. E. Gautrey, and R. Bailey. Comparison of flight test data with a computational fluid dynamics model of a Scottish Aviation Bulldog aircraft. *Aeronautical Journal*, 117:1273–1291, 2013.

[6] P. J. Roache. *Verification and Validation in Computational Science and Engineering*. Hermosa, New Mexico, USA, 1998.

[7] ESDU. Mean forces, pressure and flow field velocities for circular cylindrical structures; single cylinder with two-dimensional flow. Technical Report 80025, UK, 1986.

[8] S. F. Hoerner. *Aerodynamic Drag*. Otterbein Press, OH, USA, 1951.

[9] G. K. Batchelor. *An Introduction to Fluid Dynamics*. Cambridge University Press, UK, 1967.

[10] D. J. Acheson. *Elementary Fluid Dynamics*. Clarendon Press, UK, 1990.

[11] T. Kawamura, M. Hiwada, T. Hibino, I. Mabuchi, and M. Kumada. Flow around a finite circular cylinder on a flat plate. *JSME*, 27(232-10), 1984.

[12] E. Achenbach. Distribution of local pressure and skin friction around a circular cylinder in cross-flow up to Re = 5×10^6. *Journal of Fluid Mechanics*, 34(34), 1968.

[13] V. L. Streeter and E. B. Wylie. *Fluid Mechanics*. McGraw-Hill, NY, USA, 1975.

[14] F. T. Lynch. *Transonic Flow Aircraft Design*. Douglas Aircraft Company, 1982.

[15] O. Gur, W. H. Mason, and J. A. Schetz. Full-configuration drag estimation. *Journal of Aircraft*, 47(4):1356–1367, 2010.

[16] S. F. Hoerner. *Fluid Dynamic Drag*. Hoerner Fluid Dynamics, CA, USA, 1965.